4-2-2020

Asymmetric Imides as Electrolyte Additive for Lithium-Ion Batteries with NCM111 Cathode

Simon Weigel

Lea Eisele

Petra Klose

Brett L. Lucht

Witali Beichel

See next page for additional authors

Authors

Simon Weigel, Lea Eisele, Petra Klose, Brett L. Lucht, Witali Beichel, and Ingo Krossing

Asymmetric Imides as Electrolyte Additive for Lithium-Ion Batteries with NCM111 Cathode

Simon Weigel,[a] Lea Eisele,[a] Petra Klose,[a] Brett Lucht,[b] Witali Beichel,[a] and Ingo Krossing*[a]

The synthesis, spectroscopic and electrochemical characterization of $Li[N(SiMe_3)(SO_2R^F)]$ ($R^F = CF_3$, n-C_4F_9) as well their behavior as electrolyte additive in lithium ion batteries (LIBs) is reported. The lithium salts were obtained by deprotonation of the corresponding acids $HN(SiMe_3)(SO_2R^F)$ with n-butyllithium in n-pentane. The electrochemical investigations suggested potential as additives for LIBs. Thus, NCM111/graphite cells ($NCM111 = Li[Ni_{0.33}Co_{0.33}Mn_{0.33}]O_2$) with LP57 as electrolyte (LP57 = 1.0 M $LiPF_6$ in EC/EMC 3:7) were built to test the performance. Cells with $Li[N(SiMe_3)(SO_2R^F)]$ as additives show coulombic efficiencies of over 99.6%, less capacity fading over 55 cycles and a significantly lower cell impedance built up.

1. Introduction

Lithium-ion batteries (LIBs) are indispensable in today's everyday lifetime and play roles in portable devices as well as for the demand of electric vehicles. Since the 1990s lithiated graphite as anode material, $Li(Ni_xCo_yMn_z)O_2$ (NCM; $x+y+z=1$) as cathode active material (CAM) and a mixture consisting of $LiPF_6$ and alkyl carbonates as electrolyte became state-of-the-art.[1–3] The CAMs based on Ni- or Mn-rich compounds arose as derivatives of $LiCoO_2$ (LCO) used already in the first LIBs. Ni and Mn help to increase the capacity and improve the stability of the layered CAM.[4] Nevertheless, the limited thermal and chemical stability of the conducting salt $LiPF_6$ leads to problems due to the formation of LiF and PF_5, followed by the reaction with trace water yielding HF and OPF_3.[3,5] Electrolyte additives are able to improve the battery performance by formation of a solid electrolyte interphase (SEI) on the anode or a cathode electrolyte interphase (CEI) on the cathode side.[6–9] The SEI has been part of research for many decades and today vinylene carbonate (VC) and fluoroethylene carbonate (FEC) are the most investigated and best understood electrolyte additives and became state-of-the-art in LIBs.[10–13] Only in recent years, the focus has been more directed towards the investigation of the CEI.[6,12,14] The NCM-CAMs charged to high voltage, experience by interaction with the electrolyte transition metal dissolution, oxygen loss, electrolyte decomposition and reactions at the cathode-surface / electrolyte interface.[15] Therefore, electrolyte additives can be used that induce formation of a protective CEI and protect the alkyl carbonate based electrolyte from decomposition at high oxidation potential.[4,16] CEIs should be permeable for lithium ions, but inhibit the electron transport and further decompositions or reactions with the electrolyte. For example, some silicon based additives may improve long time stability and safety, decrease capacity fading and decomposition of the electrolyte by acting as H_2O and HF scavenger.[17–21] Several other electrolyte additives based on borates (e.g. tris (trimethylsilyl)borate **3**), phosphates, phosphites (e.g. tris (trimethylsilyl)phosphite **4**) and sulfur compounds (e.g. 1,3,2-dioxathiolane 2,2-dioxide **6**) were investigated in the literature showing both CEI and SEI formation (Scheme 1).[19,22–41]

However, there is still a desire to find a replacement for $LiPF_6$ as an electrolyte salt, due to the problems and risks mentioned above. Candidates are Lithium bis(trifluoromethanesulfonyl)imide (LiTFSI) and Lithium bis(fluorosulfonyl)imide (LiFSI) respectively asymmetric perfluoroalkylsulfonylimides, whether as pure conductive salt, as a combination (**5**) with lithium bis(oxalate)borate (LiBOB) or as additive in ionic liquid electrolytes.[28,42–63] Further, Lithium-cyclo-difluoromethane-1,1-bis(sulfonyl)imide (LiDMSI, **7**), as a representative of these perfluoroalkylsulfonylimides, shows amongst other things the formation of a CEI and a decrease of resistance in LIBs with $LiPF_6$ based electrolytes (Scheme 1).[16,20] Thus, in this work the two asymmetric lithium-imides **1** and **2** were synthesized and investigated as electrolyte additives. They combine on one side a silyl group with potential H_2O and HF scavenger properties to improve cycling stability and on the other side a perfluoroalkylsulfonyl group for CEI formation and decreased resistance built up.

[a] S. Weigel, L. Eisele, P. Klose, Dr. W. Beichel, Prof. Dr. I. Krossing
Institut für Anorganische und Analytische Chemie and Freiburger Materialforschungszentrum (FMF)
Albert-Ludwigs-Universität Freiburg
Albertstraße 21, 79104 Freiburg im Breisgau
Stefan-Meier-Straße 21, 79104 Freiburg im Breisgau, Germany
E-mail: krossing@uni-freiburg.de
[b] Prof. Dr. B. Lucht
Department of Chemistry
University of Rhode Island
Kingston, RI 02881, USA

Supporting information for this article is available on the WWW under https://doi.org/10.1002/celc.202000277

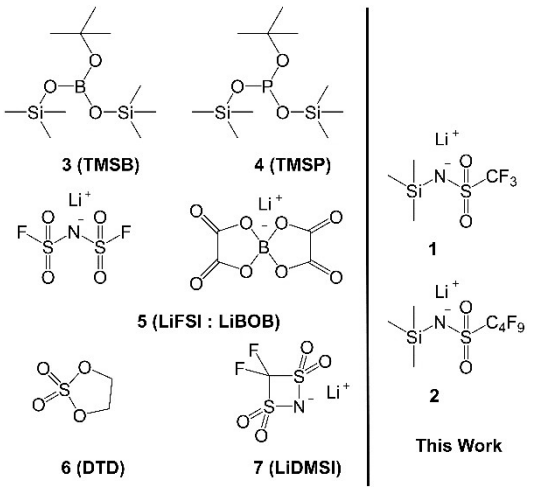

Scheme 1. Selection of cathode electrolyte interphase forming additives, tris (trimethylsilyl)borate (TMSB), tris(trimethylsilyl)phosphite (TMSP), 1,3,2-dioxathiolane 2,2-dioxide (DTD) and lithium-cyclo-difluoromethane-1,1-bis-(sulfonyl)imide (LiDMSI), mixture of lithium bis(fluorosulfonyl)imide (LiFSI) and lithium bis(oxalate)borate (LiBOB) and in this work presented asymmetric lithium-imides **1** and **2**.

2. Results and Discussion

2.1. Syntheses and Characterization

Literature known[64] Li[N(SiMe$_3$)(SO$_2$CF$_3$)] **1** and novel Li[N(SiMe$_3$)(SO$_2$C$_4$F$_9$)] **2** were prepared by the reaction of the corresponding acids HN(SiMe$_3$)(SO$_2$R^F) (R^F = CF$_3$, *n*-C$_4$F$_9$) with *n*-butyllithium in *n*-pentane in yields exceeding 99%. The compounds were investigated by multinuclear NMR spectroscopy (^{1}H, ^{7}Li, ^{19}F, ^{29}Si) and all expected signals (Electronic Supporting Information ESI: Figure S1 to S9) were detected and a purity of at least 99% was established. FT-IR (ESI: Figure S10, S11) confirmed the successful complete deprotonation of the starting material. Electrospray-ionization mass spectrometry (ESI: Figure S12, S13) showed in addition to the molecular ion peaks for **1** (m/z = 220) and **2** (m/z = 370), also one aggregate ion for **1** (m/z = 447, [Li{N(SiMe$_3$)(SO$_2$CF$_3$)}$_2$]$^-$), but two aggregate ions for **2** (m/z = 747 [LiA$_2$]$^-$, 1124 [Li$_2$A$_3$]$^-$, A = [N(SiMe$_3$)(SO$_2$C$_4$F$_9$)]$^-$). The thermogravimetric analysis (Figure 1 and 2) proved thermal stability at least

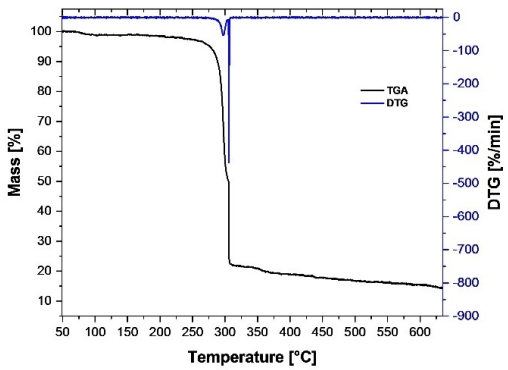

Figure 1. TGA (black) and DTG (blue) of Li[N(SiMe$_3$)(SO$_2$CF$_3$)] **1**.

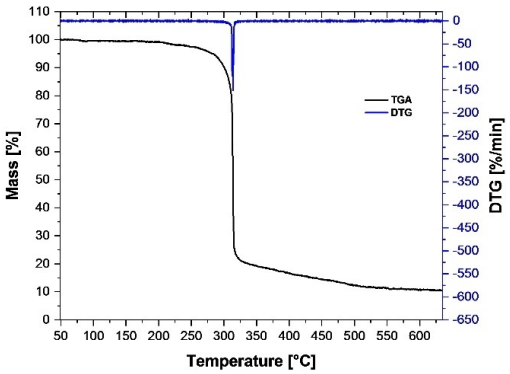

Figure 2. TGA (black) and DTG (blue) of Li[N(SiMe$_3$)(SO$_2$C$_4$F$_9$)] **2**.

up to 280 °C for both, **1** with a T_{onset} of 297 °C and **2** with a T_{onset} of 312 °C. We think due to the thermal stability and non-volatility of the solid additives, no negative impact on the flammability should be introduced to the investigated electrolyte, if compared to LP57 at least. Since additives **1** and **2** as a solid show no decomposition below 280 °C and lithium ion complexation by the solvent of the electrolyte is to be expected, a reduction in flammability can even be assumed due to the further decreased solvent vapor pressure.

2.2. Conductivity

Compounds **1** and **2** in 3:7 EC/EMC (L57) exhibited overall a very low conductivity with a maximum at room temperature at 522 µS cm^{-1} for the CF$_3$ derivate and 397 µS cm^{-1} for the C$_4$F$_9$ derivate (Figure 3). It should be noted that 0.3 mol L^{-1} is the highest concentration for both compounds to get a clear solution in L57.

These two facts indicate the high tendency of **1** and **2** towards ion pairing, as potentially induced by the structure of the anions. In the two additives used, there is only one sulfonyl group, which delocalizes the negative charge via a –M effect. In

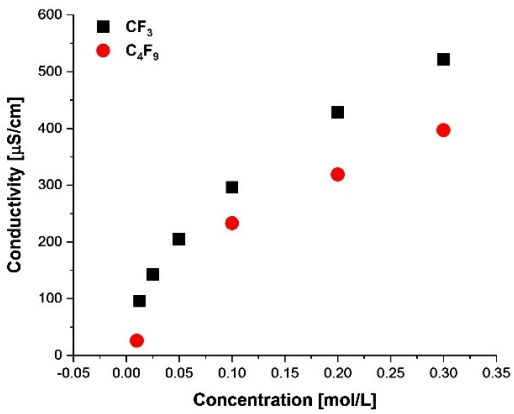

Figure 3. Concentration dependent conductivity measurements of Li[N(SiMe$_3$)(SO$_2$CF$_3$)] **1** and Li[N(SiMe$_3$)(SO$_2$C$_4$F$_9$)] **2** in L57 (EC/EMC 3:7) at 25 °C. 0.3 M is the maximum solubility of both compounds in L57.

comparison, $LiNTf_2$ ($Li[N(SO_2CF_3)_2]$) has two sulfonyl groups, which consequently delocalize the negative charge better over the entire anion. This leads to a high conductivity of 9 mS cm^{-1} [65]Klicken Sie hier, um Text einzugeben. and better solubility resulting in less ion pairing. Thus, the hyperconjugation induced by the $SiMe_3$-group does not compensate for the –M effect. Hence, any potential use as supporting electrolyte salt would be futile, and only additive testing was meaningful.

2.3. Electrochemical Testing

2.3.1. Cyclic voltammetry

The cyclic voltammograms of 0.1 M **1** and 0.1 M **2** in 1.0 M $LiPF_6$ in 3:7 (wt.%) EC/EMC (LP57) in the range of 0 to 5 V (0-3 V glassy carbon electrode, 3–5 V platinum electrode) vs Li/Li^+ were recorded (Figure 4). For **1** it suggested a redox stability in the range of 1 to 4.5 V vs Li/Li^+ and shows a rather slow drop for the anodic scan (4.5 to 5 V) from the 1st to the 5th cycle. For **2** the measured current drops both from 0 to 1 V and rather pronounced from 3.5 to 5 V from the 1st to the 5th cycle. This might indicate a passivation effect.

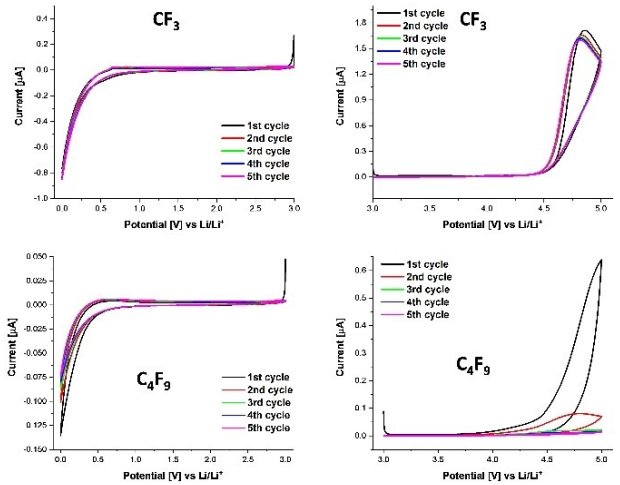

Figure 4. Cyclic voltammograms of the first five cycles of 0.1 M $Li[N(SiMe_3)(SO_2CF_3)]$ **1** in LP57 (above) and of 0.1 M $Li[N(SiMe_3)(SO_2C_4F_9)]$ **2** in LP57 (below) in the range of 0 to 3 V (glassy carbon electrode) vs Li/Li^+ (left) and 3 to 5 V (platinum electrode) vs Li/Li^+ (right).

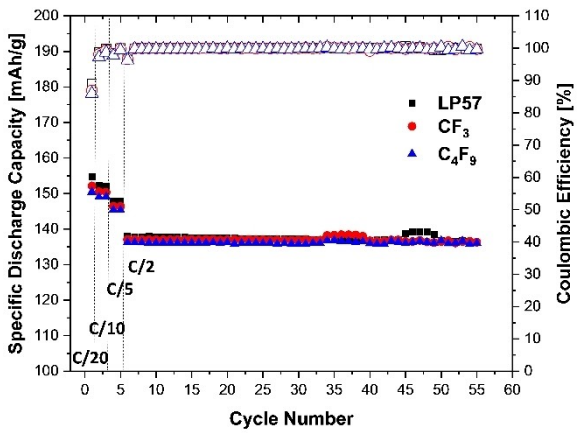

Figure 5. Average discharge profile measured at 25 °C with C/2 and coulombic efficiencies for duplicate cells with 0.25 wt.% of $Li[N(SiMe_3)(SO_2CF_3)]$ **1** and 0.25 wt.% $Li[N(SiMe_3)(SO_2C_4F_9)]$ **2** added to LP57 as well as pure LP57 as a reference. Formation cycles: one at C/20, two at C/10, and two at C/5.

2.3.2. Cell tests with 0.25 wt.% of 1 and 2 as additive

Compounds **1** and **2** were investigated as additives in NCM/graphite cells using galvanostatic cycling between 3.0 and 4.2 V at 25 °C. The electrolyte was composed of 0.25 wt.% **1** or **2** in LP57. The specific discharge capacities and coulombic efficiencies of cells with pure LP57 and with added 0.25 wt.% additive **1** or **2** as electrolyte show an almost equal curve progression over 55 cycles (Figure 5). The initial specific discharge capacity at a C-rate of C/20 is 152 mAh g^{-1} for **1** and 150 mAh g^{-1} for **2** and minimally lower than for pure LP57 (154 mAh g^{-1}). For a C-rate of C/2, the specific discharge capacity of cells with pure LP57 decreases over 50 cycles from 138 to 136 mAh g^{-1}, whereas with additive **1** it drops from 137 to 136 mAh g^{-1} and with additive **2** it stays at 136 mAh g^{-1}. The loss of specific discharge capacity with respect to the 1st cycles after formation and 50 cycles at C/2 is 11.0% for the cells with pure LP57, but only 9.9% with **1** and only 9.3% for **2** as additives.

These observations indicate a slightly better long time cycling stability by using additive **1** and more so **2** at C/2 compared to pure LP57. The coulombic efficiency in the first cycle is with 87% for **1** and 86% for **2** a little bit lower than for pure LP57 (89%) and might indicate CEI formation. After the formation cycles, cells including additives **1**, **2** or pure LP57 showed a similar progression of the coulombic efficiency at C/2 and ended all with a value of over 99.6%. The voltage profiles of the initial charge/discharge capacities of cells at C/20 with additives **1** and **2** as well as for pure LP57 show superimposable curve progressions (Figure 6a). The first cycle specific discharge capacity is with 152 mAh g^{-1} for **1** and 150 mAh g^{-1} for **2** lower by 1.9% and 3.2% compared to pure LP57 (155 mAh g^{-1}) (Figure 6b). By contrast, upon cycling at C/2 (Figure 6e), this capacity reduction with respect to cells with pure LP57 shrinks to only 0.7% for **1** and 1.4% for **2**. The dQ/dV plot exhibits a slight shift to higher voltage for the first oxidation peak at 3.5 V (Figure 6c).

There is also a slight increase of the height of the peak in going from pure LP57 (605 mAh/gV) to **2** (646 mAh/gV) and **1** (647 mAh/gV). Both may speak for CEI formation. The voltage profiles after the 10th cycle at C/2 display for both additives **1** and **2** identical profiles compared to that of LP57 (Figure 6d). The dQ/dV plot shows completely equal curve progressions suggesting no interference of the additive with the cathode active material.

The impedance measurements showed for both additives **1** and **2** as well as pure LP57 two semicircles (Figure 7). The first semicircle related to the surface film exhibits as only difference the by 13% lower starting resistance in the presence of additive

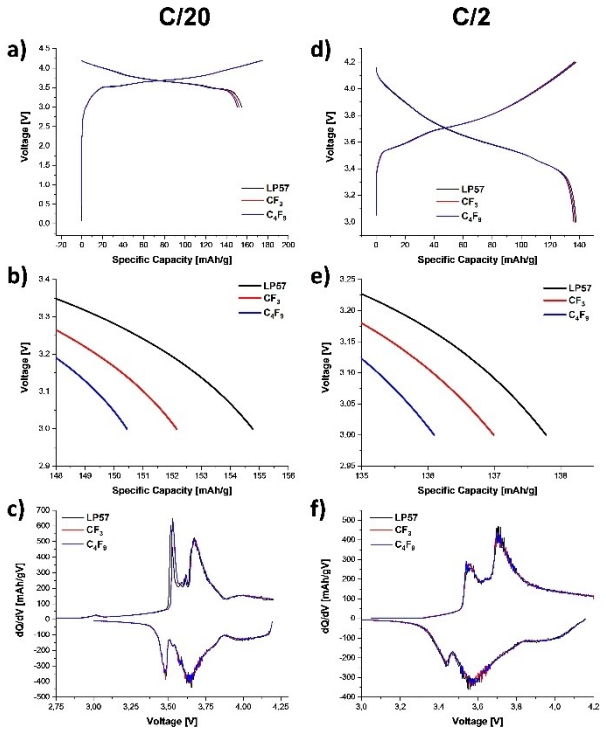

Figure 6. a) Voltage profiles of the 1st cycle at a C-rate C/20 of cells with 0.25 wt.% additive Li[N(SiMe$_3$)(SO$_2$CF$_3$)] **1**, 0.25 wt.% Li[N(SiMe$_3$)(SO$_2$C$_4$F$_9$)] **2** and pure LP57. b) Display detail of a). c) d*Q*/d*V* plot of cells after the 1st cycle at C/20 in the presence of **1**, **2** as well as in pure LP57. d) Voltage profiles after the 10th cycle at a C-rate C/2 of cells with 0.25 wt.% additive Li[N(SiMe$_3$)(SO$_2$CF$_3$)] **1**, 0.25 wt.% Li[N(SiMe$_3$)(SO$_2$C$_4$F$_9$)] **2** and with pure LP57. e) Display detail of d). f) d*Q*/d*V* plot of cells after the 10th cycle at C/2 in the presence of **1**, **2** as well as in pure LP57.

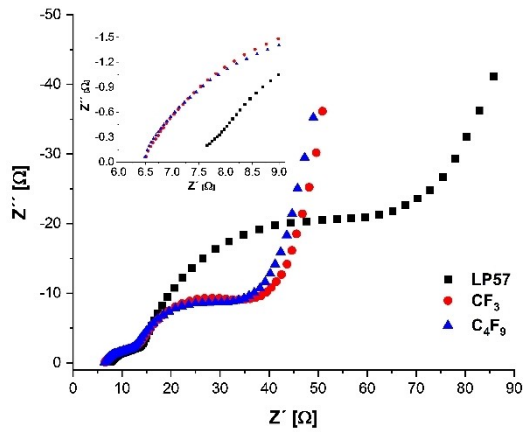

Figure 7. Nyquist plot of cells with 0.25 wt.% additive Li[N(SiMe$_3$)(SO$_2$CF$_3$)] **1**, Li[N(SiMe$_3$)(SO$_2$C$_4$F$_9$)] **2** and in pure LP57 based on measurements at a constant potential of 0 V with an amplitude of 10 mV after the 55th cycle. The inset displays a zoom to the Z′ region between 6 and 9 Ω.

1 (6.5 Ω) and **2** (6.5 Ω), if compared to pure LP57 (7.6 Ω). This finding indicates that both additives decrease the resistance of the electrolyte. Also the charge transfer resistance (CT-resistance), related to the second semicircle, with **1** and **2** as additive displays an explicitly lower resistance in comparison to pure LP57. The CT-resistance drops from 60 Ω for pure LP57 to 35 Ω in the presence of **1** and 31 Ω with **2**. Favorably, this led to nearly a halving of the CT-resistance by using only 0.25 wt % of additive **2**. We think that the improved capacity fading and lower resistance could be due to the additives **1** and **2** acting as H_2O and HF scavengers, which thus induce less electrolyte decomposition and reduced impedance built up.

2.4. Surface Characterization of the NCM111 Electrodes after Cycling

Electrodes of cells after the 55th cycle measured at a C-rate of C/2 and cycled with pure LP57, 0.25 wt.% additive **1** and **2** as well as fresh NCM111 electrodes were investigated using ex-situ XPS surface analysis (Table 1; ESI: Figures S16 to S18). The concentration of surface carbon decreases compared to pure LP57 for both additives (**1** and **2**), with fresh NCM111 having the lowest carbon content. The fresh NCM111 shows a nitrogen content, which can be explained by *N*-methyl-2-pyrrolidone fused for the cathode tape preparation. Compared to this, cycled NCM111 with LP57 exhibits a lower nitrogen concentration due to deposits of electrolyte decomposition and the limited penetration depth of XPS. Both additives **1** and **2** show an increase of 0.7 % compared to LP57. The concentration of surface sulfur exhibits for the additives in comparison to LP57 a comparable increase like for nitrogen of 0.5 to 0.6 %. Oxygen again shows an increase of at least 1.4 %, which fits to the 1 : 1 : 2 chemical composition N–SO_2 of the additives **1** and **2**. Due of the known amounts and proportions of nitrogen, sulfur and oxygen found on the CAM of the cells cycled with pure LP57 acting as a reference, the higher contents of these elements determined to reside on the CAMs being exposed to the additives have to come from the very reaction of additives 1 and 2 with the CAM in the course of the cycling. Thus, the surface compositions of the electrodes with additives **1** and **2** speak for formation of a protecting cathode electrolyte interface (CEI). Since all cycled electrodes exhibit a higher fluorine concentration than the fresh NCM111, but there is no clear trend observable, it is unclear whether the perfluoroalkyl groups are part of the CEI. The increase of the fluorine concentration among both additives may result from the longer perfluoroalkyl chain length, but does not explain the decreasing carbon concentration. The decrease of the fluorine concentration of **1** to LP57 may be an effect of less electrolyte decomposition combined by a thinner formed CEI. Thus, it appears a decomposition of the additives **1** and **2** has to take

Table 1. Relative atomic concentration of selected elements determined by ex-situ XPS surface analysis of electrodes of fresh NCM111, cycled with pure LP57 and cycled with 0.25 wt.% additive Li[N(SiMe$_3$)(SO$_2$CF$_3$)] **1** and Li[N(SiMe$_3$)(SO$_2$C$_4$F$_9$)] **2** after the 55th cycle at C/2.

	C 1s	N 1s	O 1s	F 1s	S 2p
NCM111 fresh	62.0	1.2	12.0	24.6	0.2
NCM111 with LP57	57.2	0.4	11.6	30.5	0.3
0.25 wt.% CF_3	55.8	1.1	13.8	28.4	0.8
0.25 wt.% C_4F_9	53.4	1.1	13.0	31.6	0.9

place and only nitrogen-sulfur-oxygen-structure elements in a stoichiometric ratio of 1:1:2 were incorporated in the CEI of the cathode material.

3. Conclusions

Known Li[N($SiMe_3$)(SO_2CF_3)] **1** and novel Li[N($SiMe_3$)($SO_2C_4F_9$)] **2** were synthesized, fully characterized by NMR, FT-IR, mass spectrometry and TGA and tested as electrolyte additives (0.25 wt.%) in NCM111/graphite LIB cells with LP57 as electrolyte. The electrochemical investigation displayed no effect on the coulombic efficiency after 55 cycles. Generally, both additives (**1** and **2**) show slightly lower initial discharge at C/20 of maximal 5 mAh/g compared to pure LP57 and only 2 mAh/g at C/2. By using the additives, the decrease of specific discharge capacity at C/2 over 50 cycles can be minimized. Compared to the first cycles, the capacity of cells with pure LP57 dropped by 11.0%, while those with **1** only by 9.9% and that with **2** only by 9.3%. Referring only to the C/2 cycles, only the cells with additive **2** showed virtually no capacity loss. Since the d*Q*/d*V* plots show a shift of the first oxidation peak at 3.5 V to higher voltage and XPS measurements of the cycled cells suggest N-, S- and O-uptake from the additives, apparently a favorable CEI-formation did occur. Thus, initial EIS measurements and those after 55 cycles exhibit for both additives a greatly decreased resistance compared to the pure LP57 cells. Further, the charge transfer resistance can be nearly halved compared to pure LP57 using additives **1** or **2**. All in all the chain length shows only a small effect on the electrochemical performance in cells. In conclusion, asymmetric imides as Li[N($SiMe_3$)(SO_2R^F)] ($R^F = CF_3$, *n*-C_4F_9) are suitable electrolyte additives for LIBs to improve battery performance by decreasing the capacity fade and resistance, which may result from the potential H_2O and HF scavenger properties of the $SiMe_3$ group and the demonstrated generation of a CEI via the perfluoroalkylsulfonyl group.

Experimental Section

General methods and materials

All syntheses and measurements were done under Argon atmosphere using standard Schlenk techniques or inside a glovebox (GS Glovebox or M. Braun, O_2 and H_2O content <1 ppm). Deuterated solvents were dried over CaH_2 and subsequently distilled. *n*-Pentane with a water content <4 ppm was used. NMR measurements were performed on Bruker Avance II+ WB 400 MHz and Avance III HD 300 MHz spectrometers and used for determination of purity. Chemical shifts were calibrated against the chemical shift of the residual solvent peak of CHD_2CN. A Bruker Alpha instrument with a Platinum ATR unit (diamond) was used for FT-IR measurements and evaluated with the OPUS 7.5 software (Bruker Optic GmbH). TGA was performed on a Netzsch STA 409 C/CD under nitrogen atmosphere with an empty Al_2O_3 crucible as reference. For mass spectrometry, an Advion expression L electron spray ionization mass spectrometer (ESI-MS, capillary temperature 250 °C, source voltage 30 V, source voltage dynamic 0 V, gas temperature 250 °C, ESI voltage 2500 V) was used. A Mettler Toledo SevenMulti™ conducting meter with a Mettler Toledo inLab710 4-pin platinum electrode was used for conductivity measurements. For cyclovoltametric measurements, a Methrom potentiostat Autolab PGSTAT101 with glassy carbon electrode (surface area 0.0628 cm^2, 0–3 V) and a platinum electrode (surface area 0.0157 cm^2, 3–5 V) as working electrode as well as lithium foil (BASF) as reference and counter electrode was used with the NOVA 1.8 software.

Preparations

Li[N($SiMe_3$)(SO_2CF_3)] **1**: Following the report by Chen et al.,[64] the synthesis proceeded from a mixture of HN($SiMe_3$)(SO_2CF_3) (6.1 g, 27 mmol) and *n*-pentane (200 mL) at 263 K. To this mixture, *n*-butyllithium (11 mL, 27 mmol, 2.5 M solution in *n*-hexane) was added dropwise. The suspension was stirred at 40 °C for three hours and at room temperature overnight. After removal of all volatiles under reduced pressure, **1** was obtained as a colorless powder (6.2 g, 27 mmol, 99.6%) with a purity >99% by NMR.

^{1}H NMR (400.17 MHz, CD_3CN, 298 K): δ/ppm = 0.03 (s, $^1J_{C,H}$ = 117.9 Hz, $^2J_{Si,H}$ = 6.8 Hz, 9H, Li[N(Si(**C**H_3)$_3$(SO_2CF_3)]). ^{7}Li NMR (155.52 MHz, CD_3CN, 298 K) δ/ppm = −2.3 (s, 1Li, **Li**[N(Si(CH_3)$_3$(SO_2CF_3)]). ^{19}F NMR (376.54 MHz, CD_3CN, 298 K) δ/ppm = −80.1 (s, $^1J_{C,F}$ = 325.5 Hz, 3F, Li[N(Si(CH_3)$_3$(SO_2**C**F_3)]). ^{29}Si NMR (79.50 MHz, CD_3CN, 298 K) δ/ppm = −7.3 (s, 1Si, Li[N(**Si**(CH_3)$_3$(SO_2CF_3)]). IR (400-4000 cm^{-1}, diamond ATR, corrected): ν/cm^{-1} = 2958, 2928, 2854, 1289, 1252, 1221, 1203, 1176, 1055, 840, 769, 762, 717, 693, 619, 580, 551, 525, 494. ESI-MS (negative mode): m/z = 220 (M^-), 447 ([LiA_2]$^-$, A = [N(($SiMe_3$)(SO_2CF_3)]$^-$).

Li[N($SiMe_3$)($SO_2C_4F_9$)] **2**: To a mixture of HN($SiMe_3$)($SO_2C_4F_9$) (9.0 g, 24 mmol) and *n*-pentane (200 mL) at 263 K *n*-butyllithium (9.7 mL, 24 mmol, 2.5 M solution in *n*-hexane) was added dropwise. The suspension was stirred at 40 °C for three hours and at room temperature overnight. After removal of all volatiles under reduced pressure **2** was obtained as a colorless powder (7.9 g, 24 mmol, 99.6%) with a purity >99% by NMR.

^{1}H NMR (300.18 MHz, CD_3CN, 298 K): δ/ppm = 0.03 (s, $^1J_{C,H}$ = 117.8 Hz, $^2J_{Si,H}$ = 6.8 Hz, 9H, Li[N(Si(**C**H_3)$_3$($SO_2C_4F_9$)]). ^{7}Li NMR (116.66 MHz, CD_3CN, 298 K) δ/ppm = −2.4 (s, 1Li, **Li**[N(Si(CH_3)$_3$($SO_2C_4F_9$)]). ^{19}F NMR (282.45 MHz, CD_3CN, 298 K) δ/ppm = −81.8 (tt, 3F, Li[N(Si(CH_3)$_3$(SO_2-CF_2-CF_2-CF_2-**C**F_3)]), −114.5 (m, 2F, Li[N(Si(CH_3)$_3$(SO_2-**C**F_2-CF_2-CF_2-CF_3)]), −121.4 (m, 2F, Li[N(Si(CH_3)$_3$(SO_2-CF_2-**C**F_2-CF_2-CF3)]), −126.5 (m, 2F, Li[N(Si(CH_3)$_3$(SO_2-CF_2-CF_2-**C**F_2-CF_3)]). ^{29}Si NMR (59.64 MHz, CD_3CN, 298 K) δ/ppm = −7.4 (s, 1Si, Li[N(**Si**(CH_3)$_3$($SO_2C_4F_9$)]). IR (400-4000 cm^{-1}, diamond ATR, corrected): ν/cm^{-1} = 2962, 2943, 2901, 1351, 1291, 1279, 1254, 1229, 1210, 1199, 1152, 1136, 1073, 1026, 1007, 843, 802, 764, 752, 742, 724, 695, 684, 642, 626, 617, 591, 580, 528. ESI-MS (negative mode): m/z = 370 (M^-), 747 ([LiA_2] $^-$, A = [N($SiMe_3$)($SO_2C_4F_9$)]$^-$), 1124 ([Li_2A_3]$^-$).

Cell assembly

Coin cells of the type CR 2032 were used and assembled in a glovebox. NCM cathode tapes consisting of 93% active material Li($Ni_{0.33}Co_{0.33}Mn_{0.33}$)$O_2$ (NCM111), 3% conductive additive Carbon Super C65® and 4% poly(vinylidenedifluoride) binder (PVDF, 14 mm diameter, *BASF*®) were used as cathode electrode with an average loading of 13.54 mg cm^{-2}. Graphite anode tapes consisting of 95.7% active graphite material with 0.5% conductive additive carbon Super C65® and 3.8% binder based sodium carboxymethyl cellulose (CMC) and styrene butadiene rubber (SBR, 14 mm diameter, *BASF*®) were used as electrodes with an average loading of 7.42 mg cm^{-2}. Electrodes were dried in a vacuum oven at 110 °C for 48 hours. A three layered separator consisting of Celgard 2500 (19 mm diameter)/ GF/D (19 mm diameter, Whatman®)/Celgard 2500 (19 mm diameter) was used. 90 µL electrolyte made of 1.0 M

$LiPF_6$ in 3:7 (wt.%) EC/EMC (LP57, battery grade water content ≤ 50 ppm, *BASF®*) were used. Additives used were added as weight percentage (0.25 wt.%) relating to the total mass of the electrolyte. All cells were prepared in duplicate.

Electrochemical testing

An Arbin BT2000 battery cycler was used for constant current charge/discharge cycling. Cycling performance of NCM/graphite cells was executed in the potential range between 3.00 and 4.20 V at 25 °C. The test procedure based on a formation cycling consisting of one step with a C-rate of C/20, two with C/10, two with C/5 followed by 50 cycles at C/2 starting at open circuit voltage (OCV). After 55 cycles, electrochemical impedance spectroscopy (EIS) analyses were executed three times at 25 °C for reproducibility on a Bio-Logic potentiostat at 0% state of charge (SOC), with a perturbation of 10 mV, in a frequency range from 300 kHz to 10 mHz.

Ex-situ surface analysis

In a Glovebox, cells were disassembled, rinsed with EMC (3× 500 μL) and dried overnight at elevated temperature. A thermos K-alpha system with monochromatized Al K α radiation ($h\nu = 1486.6$ eV) under ultra-high vacuum ($8.1 \cdot 10^{-8}$ Pa) was used for X-ray photoelectron spectroscopy (XPS). A vacuum transfer vessel from *Thermo Fischer®* was used for transfer into the XPS chamber. *Thermo*'s Advantage software (Version 5.988) was used for the evaluation and the binding energy was calibrated using the C 1s peak at 284.8 eV of the orbital energy of a C–C bond of conductive carbon.

Acknowledgements

Financial support of this research by BASF SE through the framework of its Scientific Network on Electrochemistry and Batteries is gratefully acknowledged by URI and UoF. We thank Fadime Bitgül and Dr. Harald Scherer for help with the NMR spectra, Andreas Warmbold for measuring the TGA.

Conflict of Interest

The authors declare no conflict of interest.

Keywords: additives · cathode electrolyte interphase · electrochemistry · lithium-ion battery · sulfur

[1] J. B. Goodenough, K.-S. Park, *J. Am. Chem. Soc.* **2013**, *135*, 1167.
[2] J. M. Tarascon, M. Armand, *Nature* **2001**, *414*, 359.
[3] F. A. Susai, H. Sclar, Y. Shilina, T. R. Penki, R. Raman, S. Maddukuri, S. Maiti, I. C. Halalay, S. Luski, B. Markovsky, D. Aurbach, *Adv. Mater.* **2018**, *30*, 1801348.
[4] B. Han, T. Paulauskas, B. Key, C. Peebles, J. S. Park, R. F. Klie, J. T. Vaughey, F. Dogan, *ACS Appl. Mater. Interfaces* **2017**, *9*, 14769.
[5] C. L. Campion, W. Li, B. L. Lucht, *J. Fluorine Chem.* **2005**, *152*, A2327.
[6] H. Zhao, X. Yu, J. Li, B. Li, H. Shao, L. Li, Y. Deng, *J. Mater. Chem. A* **2019**, *7*, 8700.
[7] A. M. Haregewoin, A. S. Wotango, B.-J. Hwang, *Energy Environ. Sci.* **2016**, *9*, 1955.
[8] B. Deng, D. Sun, Q. Wan, H. Wang, T. Chen, X. Li, M. Qu, G. Peng, *Acta Chim. Sin.* **2018**, *76*, 259.
[9] F. An, H. Zhao, W. Zhou, Y. Ma, P. Li, *Sci. Rep.* **2019**, *9*, 14108.
[10] S. S. Zhang, *J. Power Sources* **2006**, *162*, 1379.
[11] A. Wang, S. Kadam, H. Li, S. Shi, Y. Qi, *npj Comput Mater* **2018**, *4*, 359.
[12] Y. Qian, P. Niehoff, M. Börner, M. Grützke, X. Mönnighoff, P. Behrends, S. Nowak, M. Winter, F. M. Schappacher, *J. Power Sources* **2016**, *329*, 31.
[13] H. Zhang, G. G. Eshetu, X. Judez, C. Li, L. M. Rodriguez-Martínez, M. Armand, *Angew. Chem.* **2018**, *130*, 15220.
[14] K. Abe, Y. Ushigoe, H. Yoshitake, M. Yoshio, *J. Power Sources* **2006**, *153*, 328.
[15] C. Zhan, T. Wu, J. Lu, K. Amine, *Energy Environ. Sci.* **2018**, *11*, 243.
[16] P. Murmann, B. Streipert, R. Kloepsch, N. Ignatiev, P. Sartori, M. Winter, I. Cekic-Laskovic, *Phys. Chem. Chem. Phys.* **2015**, *17*, 9352.
[17] A. S. Wotango, W.-N. Su, E. G. Leggesse, A. M. Haregewoin, M.-H. Lin, T. A. Zegeye, J.-H. Cheng, B.-J. Hwang, *ACS Appl. Mater. Interfaces* **2017**, *9*, 2410.
[18] R. Zhou, J. Huang, S. Lai, J. Li, F. Wang, Z. Chen, W. Lin, C. Li, J. Wang, J. Zhao, *Sustainable Energy Fuels* **2018**, *2*, 1481.
[19] Y.-K. Han, J. Yoo, T. Yim, *J. Mater. Chem. A* **2015**, *3*, 10900.
[20] P. Murmann, M. Börner, I. Cekic-Laskovic, M. Winter, *J. Appl. Electrochem.* **2016**, *46*, 339.
[21] R. Chen, Y. Zhao, Y. Li, Y. Ye, Y. Li, F. Wu, S. Chen, *J. Mater. Chem. A* **2017**, *5*, 5142.
[22] P. Janssen, J. Kasnatscheew, B. Streipert, C. Wendt, P. Murmann, M. Ponomarenko, O. Stubbmann-Kazakova, G.-V. Röschenthaler, M. Winter, I. Cekic-Laskovic, *J. Electrochem. Soc.* **2018**, *165*, A3525–A3530.
[23] C. Li, Y. Xue, W. Zhao, S. Li, D. Zhang, *Ionics* **2015**, *21*, 737.
[24] J. Li, L. Xing, R. Zhang, M. Chen, Z. Wang, M. Xu, W. Li, *J. Power Sources* **2015**, *285*, 360.
[25] C.-Y. Liu, Y. Yang, M. Yao, H.-T. Fang, *Energy Storage Mater.* **2019**, *18*, 148.
[26] H. Rong, M. Xu, B. Xie, X. Liao, W. Huang, L. Xing, W. Li, *Electrochim. Acta* **2014**, *147*, 31.
[27] L. Xia, S. Lee, Y. Jiang, Y. Xia, G. Z. Chen, Z. Liu, *ACS Omega* **2017**, *2*, 8741.
[28] G. Yan, X. Li, Z. Wang, H. Guo, W. Peng, Q. Hu, *J. Solid State Electrochem.* **2016**, *20*, 507.
[29] T. Dagger, C. Lürenbaum, F. M. Schappacher, M. Winter, *J. Power Sources* **2017**, *342*, 266.
[30] S. Jeong, K. C. Kim, S. R. Lee, J. Mun, *Electrochim. Acta* **2019**, *300*, 156.
[31] Q. Lei, T. Yang, X. Zhao, W. Fan, W. Wang, Le Yu, S. Guo, X. Zuo, R. Zeng, J. Nan, *J. Electroanal. Chem.* **2019**, *846*, 113141.
[32] X. Qi, L. Tao, H. Hahn, C. Schultz, D. R. Gallus, X. Cao, S. Nowak, S. Röser, J. Li, I. Cekic-Laskovic, B. R. Rad, M. Winter, *RSC Adv.* **2016**, *6*, 38342.
[33] N. N. Sinha, J. C. Burns, J. R. Dahn, *J. Electrochem. Soc.* **2014**, *161*, A1084-A1089.
[34] G. Yang, J. Shi, C. Shen, S. Wang, L. Xia, H. Hu, H. Luo, Y. Xia, Z. Liu, *RSC Adv.* **2017**, *7*, 26052.
[35] T. Yang, H. Zeng, W. Wang, X. Zhao, W. Fan, C. Wang, X. Zuo, R. Zeng, J. Nan, *J. Mater. Chem. A* **2019**, *7*, 8292.
[36] B.-J. Chae, J. H. Park, H. J. Song, S. H. Jang, K. Jung, Y. D. Park, T. Yim, *Electrochim. Acta* **2018**, *290*, 465.
[37] S. H. Lee, S. Yoon, E.-H. Hwang, Y.-G. Kwon, Y.-G. Lee, K. Y. Cho, *J. Power Sources* **2018**, *378*, 112.
[38] E. J. Park, Y.-G. Kwon, S. Yoon, K. Y. Cho, *J. Power Sources* **2019**, *441*, 126668.
[39] S. Wu, Y. Lin, L. Xing, G. Sun, H. Zhou, K. Xu, W. Fan, Le Yu, W. Li, *ACS Appl. Mater. Interfaces* **2019**, *11*, 17940.
[40] X. Zheng, W. Wang, T. Huang, G. Fang, Y. Pan, M. Wu, *J. Power Sources* **2016**, *329*, 450.
[41] M. Xu, L. Zhou, Y. Dong, Y. Chen, J. Demeaux, A. D. MacIntosh, A. Garsuch, B. L. Lucht, *Energy Environ. Sci.* **2016**, *9*, 1308.
[42] H. Han, J. Guo, D. Zhang, S. Feng, W. Feng, J. Nie, Z. Zhou, *Electrochem. Commun.* **2011**, *13*, 265.
[43] S. Itabashi, K. Suzuki, M. Takahashi, K. Takeda, WO 2017208944.
[44] S. J. Kim, U. C. Shin, M. J. Lee, M. S. Kim, E. Y. Ko, M. H. Jung, KR 2016055002.
[45] Kumiko Mie, Hizuru Koshina, Tooru Matsui, Masaki Deguchi, US7709157B2.
[46] C. H. Lee, S. K. Kim, G. Y. Kim, D. K. Yang, US 20190214681.
[47] A. Lewandowski, A. Świderska-Mocek, *J. Power Sources* **2007**, *171*, 938.
[48] A. Liu, *Ionics* **2014**, *20*, 451.
[49] S. Nakanishi, H. Koshina, WO 2006008921.
[50] X. Qin, J. Lv, L. Tao, L. Wang, CN 109411822.

[51] X. Shangguan, G. Jia, F. Li, S. Liu, G. Yang, K. Wu, Z. Wu, *Energy Technol.* **2018**, *6*, 1667.
[52] V. Sharova, A. Moretti, T. Diemant, A. Varzi, R. J. Behm, S. Passerini, *J. Power Sources* **2018**, *375*, 43.
[53] J. Sundermeyer, B. Roling, T. Linder, T. Froemling, B. Huber, EP 2314572.
[54] M. Tsurumi, H. Nagura, Y. Harada, JP 10255846.
[55] Z. Wang, Y. Cai, T. Dong, S. Chen, X. Lu, *Ionics* **2013**, *19*, 887.
[56] William M. Lamanna, Larry J. Krause, US5652072A.
[57] William M. Lamanna, Robert B. Loch, Alan D. Fanta, Steven D. Boyd, Hiroshi Shimada, Phat T. Pham, Bryan J. Johnson, US6280883B1.
[58] Y. Yang, H. Han, CN 103682444.
[59] Y. Yang, X. Zhan, H. Wan, Z. Wang, M. Xu, CN 105119017.
[60] L. Zhang, L. Chai, L. Zhang, M. Shen, X. Zhang, V. S. Battaglia, T. Stephenson, H. Zheng, *Electrochim. Acta* **2014**, *127*, 39.
[61] F. Ahmed, M. M. Rahman, S. Chandra Sutradhar, N. Siraj Lopa, T. Ryu, S. Yoon, I. Choi, J. Kim, Y. Jin, W. Kim, *J. Ind. Eng. Chem.* **2019**, *78*, 178.
[62] F. Ahmed, M. M. Rahman, S. C. Sutradhar, N. S. Lopa, T. Ryu, S. Yoon, I. Choi, Y. Lee, W. Kim, *Electrochim. Acta* **2019**, *302*, 161.
[63] C. Forestier, S. Grugeon, C. Davoisne, A. Lecocq, G. Marlair, M. Armand, L. Sannier, S. Laruelle, *J. Power Sources* **2016**, *330*, 186.
[64] T. Chen, B. S. Majumdar, *Main Group Chem.* **2016**, *15*, 375.
[65] C. W. Walker, *J. Electrochem. Soc.* **1996**, *143*, L80.

Manuscript received: February 19, 2020
Revised manuscript received: March 31, 2020
Accepted manuscript online: April 2, 2020